Structure–function subsystem models of female and male forebrain networks integrating cognition, affect, behavior, and bodily functions

Larry W. Swanson[a,1], Joel D. Hahn[a], and Olaf Sporns[b,c]

[a]Department of Biological Sciences, University of Southern California, Los Angeles, CA 90089; [b]Indiana University Network Science Institute, Indiana University, Bloomington, IN 47405; and [c]Department of Psychological and Brain Sciences, Indiana University, Bloomington, IN 47405

Contributed by Larry W. Swanson, October 13, 2020 (sent for review August 21, 2020; reviewed by Z. Josh Huang and Liqun Luo)

The forebrain is the first of three primary vertebrate brain subdivisions. Macrolevel network analysis in a mammal (rat) revealed that the 466 gray matter regions composing the right and left sides of the forebrain are interconnected by 35,738 axonal connections forming a large set of overlapping, hierarchically arranged subsystems. This hierarchy is bilaterally symmetrical and sexually dimorphic, and it was used to create a structure–function conceptual model of intraforebrain network organization. Two mirror image top-level subsystems are presumably the most fundamental ontogenetically and phylogenetically. They essentially form the right and left forebrain halves and are relatively weakly interconnected. Each top-level subsystem in turn has two second-level subsystems. A ventromedial subsystem includes the medial forebrain bundle, functionally coordinating instinctive survival behaviors with appropriate physiological responses and affect. This subsystem has 26/24 (female/male) lowest-level subsystems, all using a combination of glutamate and GABA as neurotransmitters. In contrast, a dorsolateral subsystem includes the lateral forebrain bundle, functionally mediating voluntary behavior and cognition. This subsystem has 20 lowest-level subsystems, and all but 4 use glutamate exclusively for their macroconnections; no forebrain subsystems are exclusively GABAergic. Bottom-up subsystem analysis is a powerful engine for generating testable hypotheses about mechanistic explanations of brain function, behavior, and mind based on underlying circuit organization. Targeted computational (virtual) lesioning of specific regions of interest associated with Alzheimer's disease, clinical depression, and other disorders may begin to clarify how the effects spread through the entire forebrain network model.

Alzheimer's disease | connectomics | depression | neuroinformatics | sexual dimorphisms

Developmentally, the vertebrate nervous system's central division, the neural tube, has four primary subdivisions: forebrain (FB), midbrain, hindbrain, and spinal cord (1, 2). Functionally, the mammalian FB is critical for survival of individuals and of species because it is required for the spontaneous expression of goal-directed homeostatic and reproductive behaviors (3, 4) and for coordinating specific behaviors with physiologically appropriate autonomic and neuroendocrine visceral responses (5–7). The FB may thus be viewed broadly as a biological network controlling voluntary behavior, generating associated conscious experience (cognition and affect) (8), and coordinating behavior and conscious experience with bodily functions.

Based on its diverse and critical functional roles, it is not surprising that the FB is the most differentiated mammalian nervous system part, with four traditional subdivisions (cerebral cortex [CTX], cerebral nuclei [CNU], thalamus [TH], and hypothalamus [HY]), together parceled into about half of all recognized nervous system gray matter regions (466/920 bilaterally in rat) (9). A vast literature addresses the structure–function properties of many FB regions and their axonal connections with other regions, but no conceptual model of global FB structure–function architecture has emerged to provide a basic plan and first principles for generating data-driven testable hypotheses from bottom-up and/or top-down approaches.

Network neuroscience provides tools for systematically constructing and deconstructing global models of systems architecture, most recently in terms of subsystem (module) hierarchies (10–12). For systems analysis generally, basic requirements include a parts list, an understanding of how each part works, and an account of how the parts interconnect and function as a whole. In neuroscience, the most complete analysis of the whole adult nervous system is for the two sexes of the nematode, *Caenorhabditis elegans*, with fewer than 400 neurons (parts) and on the order of 6,000 to 7,000 synapses (connections) (13, 14). Brenner and colleagues rationalized the whole nervous system approach by noting that less than a complete solution at any analysis level is modifiable by additional data at that level and by suggesting that solutions help answer two fundamental questions in neurobiology: 1) how do neurons in the embryo organize themselves into specifically interconnected structural networks and then 2) how do such networks function in the adult (13, 15)?

We have approached constructing a global adult mammalian nervous system wiring diagram—as a necessary prelude to examining how it develops and understanding how it constrains the

Significance

The forebrain is required for generating mammalian voluntary and innate behaviors. Multiresolution consensus cluster analysis generated a panoramic, hierarchical view of rat intraforebrain structure–function subsystem organization, from the top level with just two relatively independent mirror image subsystems centered on either side of the brain, to over 90 bottom-level subsystems. Each top-level subsystem has two interconnected subsystems: one includes the medial forebrain bundle and integrates instinctive survival behaviors with relevant physiological responses and affect, whereas the other uses the lateral forebrain bundle and mediates voluntary behavior control, with associated cognition. The intraforebrain network is sexually dimorphic, and targeted computational lesions of nodes implicated in human Alzheimer's disease and depression produce severe, differential, global network changes in males and females.

Author contributions: L.W.S. designed research; L.W.S. and J.D.H. performed research; L.W.S., J.D.H., and O.S. analyzed data; and L.W.S. wrote the paper with contributions from J.D.H. and O.S.

Reviewers: Z.J.H., Cold Spring Harbor Laboratory; and L.L., Stanford University.

The authors declare no competing interest.

[1]To whom correspondence may be addressed. Email: larryswanson10@gmail.com.

This article contains supporting information online at https://www.pnas.org/lookup/suppl/doi:10.1073/pnas.2017733117/-/DCSupplemental.

First published November 23, 2020.

range of adult functional dynamics—by starting with a macroconnectome, a matrix of directed and weighted axonal connections between all gray matter regions (parts) in rat, a granularity level and species where by far the most data currently exist. Because a 920 × 920 matrix of rat nervous system regions has 846,400 possible monosynaptic macroconnections (referred to below simply as connections), for practical reasons we decided initially to create separate subconnectomes for each of the central nervous system's 10 subdivisions (Fig. 1*B*), to progress from rostral to caudal, and then to add the peripheral nervous system and its interactions with the rest of the body—a neurome (16). This practical strategy also yields conceptual results because the intrinsic circuitry of each subdivision, considered as an aggregate part, can be analyzed, along with the organization of intersubdivisional connections. A top-level macroneuroscience approach is meant to provide boundary conditions (total interregional connectivity pattern) and a theoretical framework for understanding rodent nervous system organization at finer, nested levels of granularity: the set of neuron types forming a region (mesolevel), the set of individual neurons forming a type (microlevel), and the set of synapses for individual neurons (nanolevel) (17).

Network analysis now has been applied to the internal connections of CTX, CNU, TH, and HY and to connections between CTX and CNU (endbrain [EB]) and between TH and HY (interbrain [IB]) (12, 16, 18–22). Here a systematic, comprehensive database of all possible intra-FB connections was generated (by including those between EB and IB) and subjected to network analysis, preparatory to adding more caudal central nervous system parts, and the peripheral nervous system.

Results

Analysis Framework. The analysis is based on experimental pathway tracing evidence of connection presence (and weight) or absence between all 466 gray matter regions (nodes) on the right and left FB sides in our rat brain reference atlas (9) (Fig. 1 and Dataset S1 for abbreviations), described with defined vocabularies for axonal connections (23, 24) and gray matter regionalization in mammals (25, 26). Connection reports were expertly collated from the primary structural neuroscience literature (*SI Appendix, Materials and Methods*).

The number of possible intra-FB connections on one side (ipsilateral, uncrossed, or association connections) is 54,056 (233^2 – 233; intraregional connections are ignored), and the number of possible intra-FB connections to the other side (contralateral, crossed, or commissural) is 54,289 (233^2), making 216,690 possible intra-FB connections bilaterally. Because our systematic collation identified no statistically significant right–left (or strain) FB connectional differences, all ipsilateral and contralateral connections were assigned to one side, and the same dataset was used for the other side. Thus, our analysis applies to the species level (adult female and male rat, *Rattus norvegicus domestica*).

For systematic and practical data collection and analysis, the FB connection matrix (subconnectome) was divided into 64 subconnectomes (Fig. 1*C*). We already published (12, 18–22) 32 subconnectomes (or used updated versions; *SI Appendix, Materials and Methods*) involving right and left CTX, CNU, TH, and HY: 16 concern bilateral intra-CTX, intra-CNU, intra-TH, and intra-HY connections; 8 concern bilateral connections between CTX and CNU (the EB); and 8 concern bilateral connections between TH and HY (the IB). The remaining 32 subconnectomes (Fig. 1*C*, white rectangles) were collated for this analysis (intra-HY and HY > TH connection reports by J.D.H. and the rest by L.W.S.). For a comparison of collations for the same connection matrix by two experts, see ref. 19.

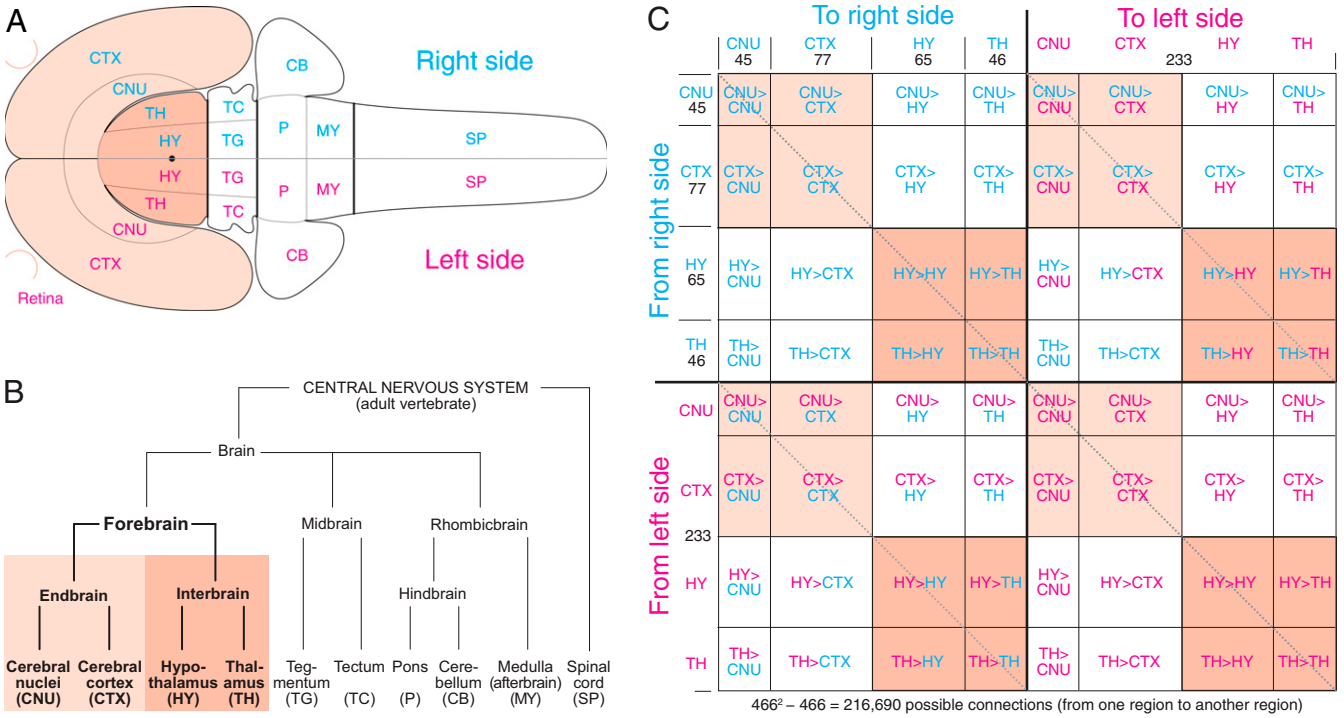

Fig. 1. Analysis strategy overview. (*A*) The right and left FB, consisting of CTX, CNU, TH, and HY (with retina) shown on a rat central nervous system flat map (28). (*B*) Hierarchy of major central nervous system subdivisions common to adult vertebrates (1, 2). (*C*) The 64 subdivision subconnectomes assembled in topographic order to create the whole FB subconnectome. Numbers indicate region number in a subconnectome or subdivision (*B*). The main diagonal (darker dashed line, upper left to lower right) indicates the connection of a region to itself, with no value in a macroconnectome where regions are black boxes. The two shorter diagonals (lighter dashed lines) parallel to the main diagonal represent homotopic crossed connections: from a region on one side of the brain to the corresponding region on the other side.

A dataset of 187,131 connection reports (≥19 columns of metadata/report) for ipsilateral and contralateral connections from the FB on one side was collated from 557 original research publications appearing since 1973, for 108,345 possible connections (with no right/left differences, doubled values are 374,262 connection reports for 216,690 possible connections for both sides). The connection reports were from 53 journals, book articles, or theses (54.3% from the *Journal of Comparative Neurology*) involving about 276 laboratories; 26.4% of the connection reports (49,374 for ipsilateral and contralateral connections arising on one side) were from the L.W.S. laboratory. Other top-producing laboratories were C. B. Saper (8,728, 4.6%), R. P. Vertes (6,334, 3.4%), J. L. Price (5,382, 2.9%), and S. J. Shammah-Lagnado (4,927, 2.6%). Overall, 31 different pathway tracing methods were used in generating connection reports; this and other metadata for each report are in Dataset S2.

Basic Connection Numbers and Data Validity. The collation identified 13,778 ipsilateral intra-FB connections as present and 38,126 as absent, a 26.5% connection density. As before (18, 22), "unclear" values are binned with "absent" values, "axons-of-passage" are binned conservatively with "weak", and "present" are binned with "moderate." In contrast, 4,091 contralateral intra-FB connections from one side were identified as present and 46,716 as absent (8.1% connection density). Thus, for each FB side, 17,869 ipsilateral and contralateral connections were identified as present, and 84,842 were identified as absent (17.4% connection density); these numbers are doubled for the complete bilateral intra-FB connection matrix (connection density is also 17.4% because no right–left differences; 95.8% of the connection reports used for analysis did not report which FB side was microinjected with pathway tracer).

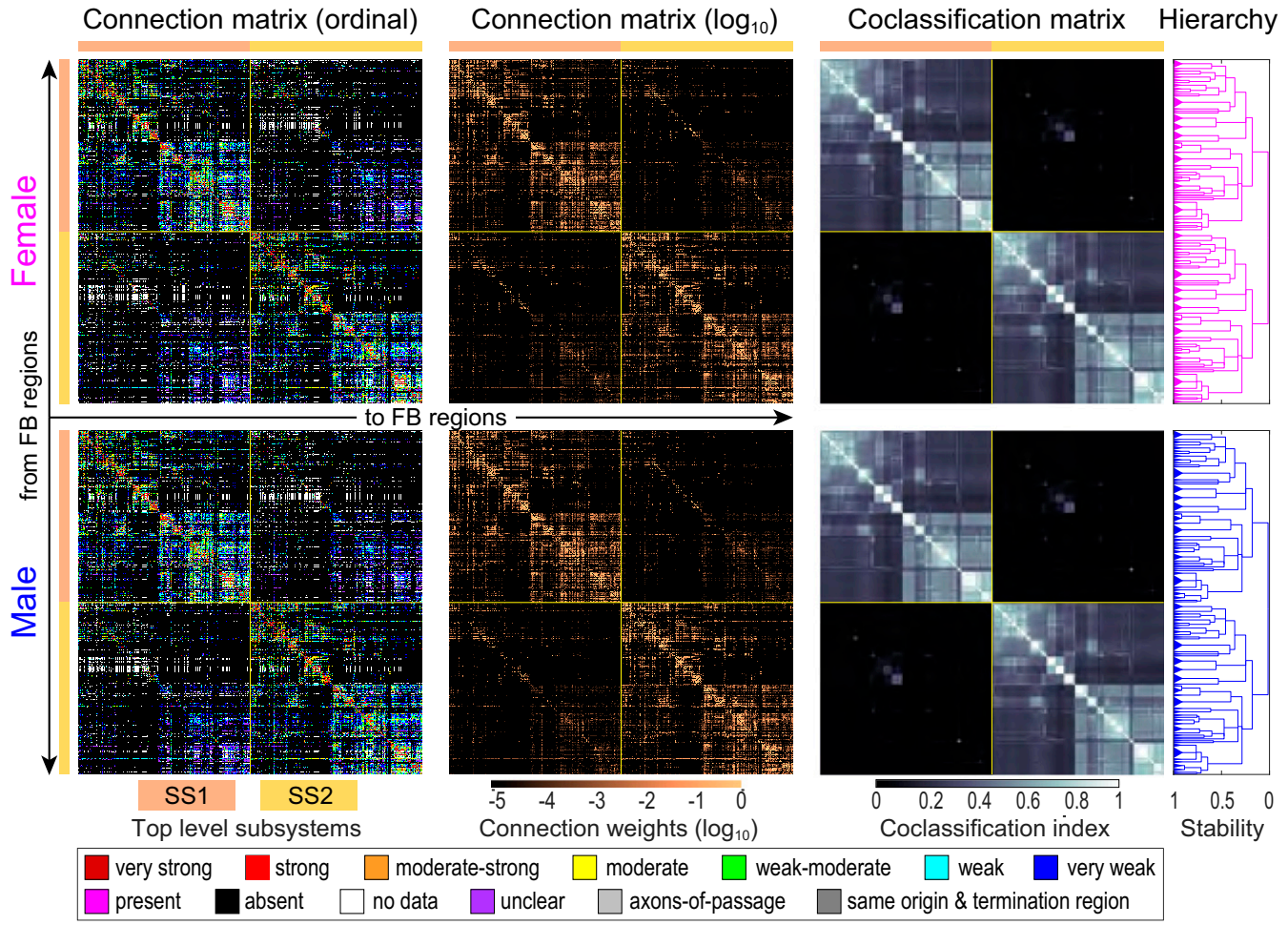

Fig. 2. Bilateral female and male rat intraforebrain macroconnectomes (FB2). Directed and weighted monosynaptic macroconnection matrices with gray matter region sequence in a subsystem arrangement derived from MRCC analysis. Collated data are represented by descriptive terms corresponding to ordinal weight values (first column; key at bottom) and then converted to binned log-weighted values (second column) for computation. MRCC of the log-weighted connection data generated coclassification matrices (third column), also represented as a hierarchal dendrogram (fourth column) for female (pink) and male (blue). Coclassification refers to how well a given connection correlates with the solutions provided by MRCC analysis. The linearly scaled coclassification index gives a range between 0 (no coclassification at any partitioning resolution) and 1 (perfect coclassification across all partitioning resolutions). Two top-level subsystems (SS1 and SS2; top left and bottom right matrix quadrants, respectively) are outlined in yellow and indicated by colored bars next to the matrices. Except for one region (retina), SS1 and SS2 are unilateral (left side or right side). In an MRCC hierarchy, the length of a particular branch set represents a distance between it and adjacent sets; this length may be interpreted as the branch set's stability (or persistence) across the entire hierarchy such that dominant solutions (branch sets more resistant to splitting) have longer branches and fleeting or unstable solutions have shorter branches. All solutions plotted in the tree survive the statistical significance level of $\alpha = 0.05$. Note that specific sexual dimorphisms are not easily discernable here; much greater magnification is required (*SI Appendix*, Fig. S3 *D* and *E* and Dataset S4*J*). For region (row and column) identity and additional details, see Figs. 5 and 6; *SI Appendix*, Fig. S3; and Datasets S3 and S4.

No published data were found for 2,152 (4.0%) of all 54,056 possible ipsilateral intra-FB connections for a matrix coverage (fill ratio) of 96.0% (Fig. 2, first column), whereas matrix coverage for contralateral connections was 93.6% (no article found for 3,482 of 54,289 possible connections). Thus, matrix coverage for all ipsilateral and contralateral connections arising in one FB is 94.8%, which also applies to the complete bilateral intra-FB connection matrix (with no right–left differences).

Assuming the connection reports representatively sample the 233-region matrix for each FB side, a complete ipsilateral intra-FB connection matrix would contain ~14,349 connections, a complete contralateral intra-FB connection matrix would contain ~4,371 connections, and the complete bilateral intra-FB connection matrix would contain 37,698 connections.

For network analysis, reported connection weight values of "no data" and "unclear" were binned with "absent" values, and all values were converted from the descriptive ordinal scale to a $\log_{10}$ scale covering five orders of magnitude, the reported range of rat connectional data (16) (Fig. 2, second column). The resulting connection densities for ipsilateral and contralateral intra-FB connections are ipsilateral, 25.5%; contralateral, 7.5%; and both ipsilateral and contralateral, 16.5% (Dataset S3). For FB regions, the range of ipsilateral and contralateral output connections (the output connection degree range) is 0 to 363 (for indusium griseum, fasciola cinerea, and bed nuclei of terminal stria strial extension, it was 0; the output connections of these regions have not been investigated with pathway tracing experiments in rat), the input connection degree range is 1 to 205, and the total (input + output) degree range is 6 to 425.

A validity metric was applied to the pathway tracing method associated with each connection report (12, 19) (*SI Appendix, Materials and Methods*). The metric uses an ordinal seven-point scale (1 to 7 indicate lowest to highest validity). Using this approach, the following average validity values were determined for the data that were used for network analysis: for connections reported to exist, ipsilateral (within one side) = 6.52, contralateral (between sides) = 6.57, and within and between sides = 6.53; for connections reported to not exist, ipsilateral = 6.20, contralateral = 6.24, and both = 6.22 (Datasets S2 and S4*O*).

Female–Male Difference. Of 216,690 possible intra-FB connections, 4/35,738 identified as present are markedly sexually dimorphic based on statistical analysis. The right and left ipsilateral connections from bed nuclei of terminal stria principal nucleus (BSTpr) to anteroventral periventricular nucleus (AVPV) are 6× stronger in males (very strong versus weak; ordinal scale), and the right and left ipsilateral connections from BSTpr to ventral premammillary nucleus (PMv) are 4× stronger in males (rated very strong versus moderate) (Datasets S2 and S3). In previous collations of intra-EB (12) and intra-IB (22) connections, no statistically significant sexually dimorphic connections were found; the four reported here are from CNU (EB) to HY (IB), and they are involved in controlling the estrous cycle and other reproductive functions (27). These established sexual dimorphisms required construction and analysis of separate female and male FB connection matrices (Fig. 2).

Subsystem Analysis. Cluster analysis is a powerful way to detect node sets more heavily connected with each other than with other node sets in a network or system. Here multiresolution consensus cluster (MRCC) analysis (11, 12) was applied to the complete bilateral (466 × 466 region) female and male FB connection matrices (FB2f and FB2m, respectively). MRCC analysis aims to detect strongly connected clusters (called communities; modules; or the synonym used here, subsystems) among the directed and weighted connections between all FB regions (nodes)—across all levels of partitioning resolution or scale (1 to 465 possible levels for FB2)—thus identifying without preconceived biases variously sized clusters that are arranged hierarchically, which generates a compact description of all nested subsystems and their interactions.

Because datasets for connections arising on FB sides 1 and 2 are identical (*Analysis Framework*), MRCC analysis of FB2f and FB2m should generate precisely symmetric subsystems across the median plane. However, because of the MRCC algorithm mechanism, the presence of extremely strong crossed homotopic connections can prevent their symmetric division and allocation. Using an approach described previously (22), we found that symmetric MRCC solutions (Fig. 2) were obtained only after omitting the right and left nucleus of lateral olfactory tract dorsal cap (NLOT3), a CTX region with a very strong crossed homotopic connection that should be viewed as a tiny top-level subsystem, although it is not considered further here. Thus, analysis proceeded on a 464 × 464 FB2 connection matrix.

The major top-level MRCC solutions for FB2f and FB2m were identical and very simple (Fig. 2): two mirror image subsystems (SS1 and SS2), with all but one of the 232 regions (without NLOT3) in each subsystem located unilaterally. The one exception is the contralateral retina, an embryological HY outgrowth with a very weak ipsilateral connection in rat. Furthermore, SS1 and SS2 are relatively weakly interconnected: weighted connection densities (WCDs) within SS1 and SS2 are 12.7× greater than the WCD between them (Fig. 3*A*). This result suggests that when viewed isolated from the rest of the nervous system, the right and left FB sides operate relatively independently, with mostly weak interactions between them. The two–top-level subsystem solution for FB2 contrasts with the six–top-level subsystem solution reported for the bilateral intra-CTX (CTX2) network (19).

Structural Subsystem Hierarchy. As MRCC analysis proceeds iteratively from two top-level subsystems (SS1f,m and mirror image SS2f,m, just described) through lower-level (nested) subsystems, a scaled cluster tree reveals the full subsystem hierarchy (Fig. 2, fourth column). Again, quite simply, SS1f,m and SS2f,m split into two second-level subsystems (Fig. 3*B*), and each second-level subsystem then splits into three third-level subsystems. Three second-level subsystem interaction features are obvious (Fig. 3*B*). First, relatively balanced and strong bidirectional connections occur between SS1.1 and SS1.2 (and mirror image SS2.1 and SS2.2). Second, similarly strong crossed homotopic connections occur between SS1.1 and SS2.1, whereas crossed homotopic connections between SS1.2 and SS2.2 are about a third as strong. Third, crossed heterotopic connections in the network are extremely weak.

What are the regional members of these subsystems, and how are they distributed spatially within the FB? Instead of distributing spatially in a checkerboard pattern, the region sets forming the first- through third-level subsystems tend to aggregate spatially in CTX, CNU, TH, and HY, as viewed schematically on a flat map (28) and an atlas (9) of transverse section maps (Figs. 3*C* and 4). Visual inspection suggests a clear although partly incomplete dual aggregation pattern—one predominating in CTX and dorsal TH (Figs. 3*C* and 4, blue), and the other predominating in HY (Figs. 3*C* and 4, red), with CNU participating significantly in both aggregates. The functional implications of this broad aggregation pattern are considered below.

Conversely, the bottom level of the FB2f hierarchy has 92 subsystems with 46 mirror image subsystems in each top-level subsystem (SS1f and SS2f) (Fig. 2). Each bottom-level subsystem is a small set of FB regions (range 2 to 15 and mean 5.1) more densely connected intrinsically than with other subsystems, and going up the hierarchy, some sets associate more closely with each other than with other sets, as measured by the hierarchy stability (persistence) index for each branch (Fig. 2, fourth column). The tendency for subsystem regions to form spatially

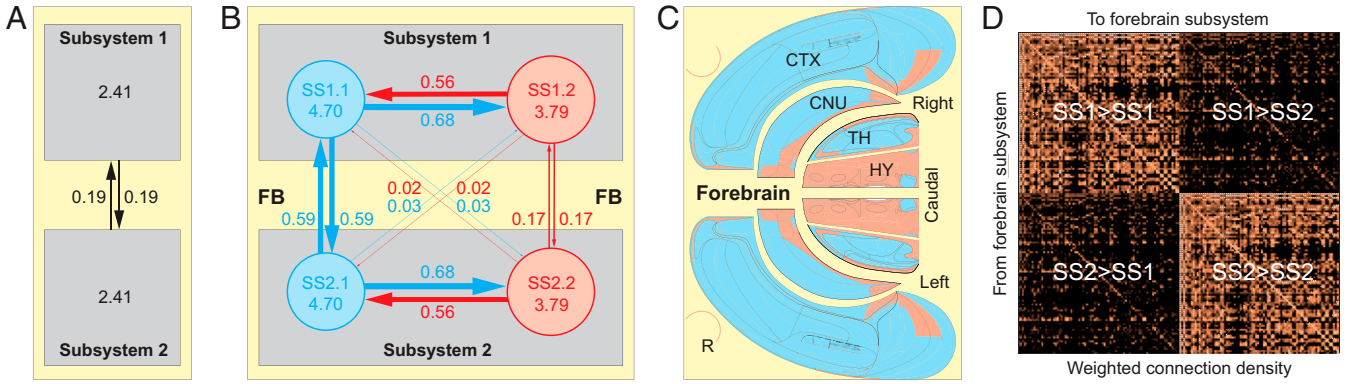

Fig. 3. High-level bilateral FB subsystem interactions. (*A*) The two top-level subsystems (SS1 and SS2) are mirror images, each having all but 1 (retina [R]) of its 233 regions on one side of the brain (Fig. 2, third column). As measured by WCD (aggregate connection strength/total number of regions, ×100), their intrinsic connections are 12.7× stronger than connections between them (4.82 vs. 0.38). (*B*) Schematic diagram of second-level interaction strengths (line thickness approximately proportional to WCD value). (*C*) Spatial distribution of the first (blue; SS1.1 and SS2.1) and second (red; SS1.2 and SS2.2) second-level subsystems displayed on an expanded flat map (Fig. 1*A*), color-coded with *B*. (*D*) Matrix of all subsystem interconnections for the FB2f network, with matrix entries recording each subsystem pair's WCD computed (as a mean across all its constituent region pairs) from data in Fig. 2, *Top* of third column. Subsystem pairs with regions in common are marked with a white circle. See *A Network of Subsystems* for details. For flat map details, see Fig. 4. Adapted from ref. 28. For ordered list of subsystems in *D*, see Figs. 5 and 6 and Dataset S4*S*. Abbreviations are in Fig. 1.

continuous masses in CTX, CNU, TH, and HY extends to the bottom level, where it applies to 71.7% of SS1 and SS2 subsystems (80.0% in SS1.1 and SS2.1 and 65.4% in SS1.2 and SS2.2). This finding of spatially contiguous subsystems suggests the hypothesis that connections do not tend to take the most direct routes within the overall FB2 network but do tend to take the most direct route within their parent subsystems.

The simplest way to explore the network hierarchy is from the bottom up: pick one of the 464 FB2f regions and note the set of regions with which it is most densely connected—its bottom-level subsystem. Then, the subsystem(s) most closely associated with this subsystem can be determined at the same or higher hierarchy levels and so on, eventually reaching the top of the hierarchy.

A Network of Subsystems. The MRCC hierarchies present rich descriptions of possible subsystem interactions. The complete FB2f hierarchy, with 2 top-level and 92 bottom-level subsystems, has 75 levels defining 166 unique subsystems (hierarchy branches, excluding right and left NLOT3 subsystem; Fig. 2 and Dataset S4 *B*, *C*, *E*, and *I*). An informative approach to potential subsystem interactions, along with the hierarchy stability index, is to compare WCDs within and between all subsystem pairs, not just at the uppermost levels (Fig. 3 *A* and *B*). For the entire FB2f hierarchy this yields a 166 × 166 matrix of WCDs within and between all subsystems (Fig. 3*D* and Dataset S4*S* for details), derived from the original connection matrix (Fig. 2) and associated with metrics for each subsystem, including number of regions, hierarchy stability index, intrinsic WCD, input/output WCD ratio, anatomical subdivision contributions, WCD with all other subsystems, and complement of reciprocal and unidirectional connections (Dataset S4 *Q* and *R*). This matrix has 27,390 ($166^2 - 166$) possible subsystem interactions, compared with 216,690 possible connections in the FB2f system, offering an abstraction or simplification level to the analysis that itself could be subjected to cluster analysis. The FB2f and FB2m MRCC hierarchies are compared below.

Hierarchical Structure–Function Subsystem Model. From a neurobiological standpoint, MRCC analysis becomes more informative when it tests the core hypotheses that 1) individual clusters, distinguished by unique structural connection sets, form stable subsystems with unique functional properties and 2) these structure–function subsystems interact within a hierarchically organized global framework (22). The utility of this approach is clarified by viewing individually each of the upper-level subsystems shown together on the flat map in Fig. 4. Some upper-level subsystems are easy to interpret: one includes just the dorsal lateral geniculate nucleus and visual cortical areas (*SI Appendix*, Fig. S1*A*), and another involves the canonical mammillary HY-anterior TH-cingulate CTX region path (*SI Appendix*, Fig. S1*H*). The other upper-level subsystems are more complex, however, and to clarify their possible significance alone, and within the entire MRCC hierarchy framework, a different strategy was used.

Based on the two core hypotheses, a functional interpretation was applied to the FB2f structural subsystem hierarchy (Fig. 2), starting at the bottom, most differentiated or specialized level and working systematically upward (Figs. 5 and 6). The literature on FB structure–function correlates is too vast to review here; for relevant literature guides, see citations in Dataset S2 and our papers on individual FB divisions (12, 18–22). For this prototype model (version 1.0), only the most established and easily summarized (if any) functional correlates (primary associations) are assigned to one or more regions in a subsystem, and remaining regions are associated with this function via their intrasubsystem connections. Our working model, like any, is selective, a simplification, and based on (and constrained by) current evidence.

Bottom-Up Example: Gustatory Subsystem. It is impractical to describe the whole FB2f structure–function hierarchy (Figs. 5 and 6) with its 35,738 connections. Instead, a generally applicable example analysis is provided: the hierarchy's first two lowest-level subsystems (Figs. 2 and 5) that are associated with the CTX gustatory area (GU) and thus presumably with taste-related functionality.

The first lowest-level subsystem (*SI Appendix*, Fig. S2 *A* and *C*) has 11 regions, including GU, and 77 of a possible 110 interregional connections, which are distributed through the CTX (5 regions), CNU (2 regions), and TH (4 regions) (for subsystem composition, see Datasets S3 and S4 *C*, *E*, and *F*). Collectively, the 11 regions in this subsystem connect more strongly with each other than with any other subsystem, prompting the hypothesis that for this particular subsystem, each constituent region associates more with taste-related functions than any other function.

By contrast, the second lowest-level subsystem (*SI Appendix*, Fig. S2 *A* and *D*) has only two regions: CTX prelimbic area (PL) and TH mediodorsal nucleus medial part (MDm), which are strongly and bidirectionally connected. The functional significance of PL, a prefrontal region, is currently vague, but because

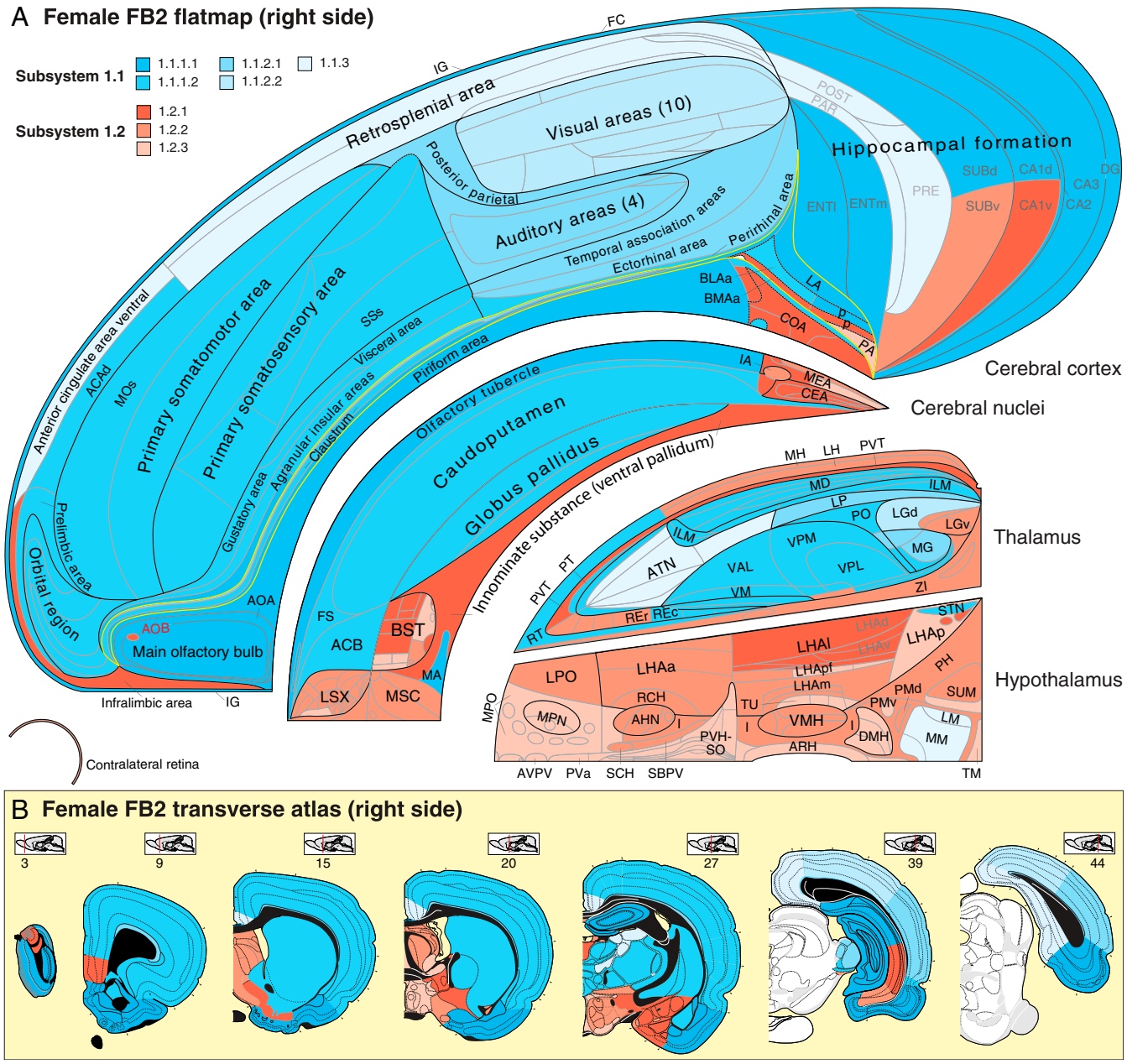

Fig. 4. (*A*) Spatial distribution of upper-level connection subsystems displayed on a flat map and (*B*) reference atlas of the right FB. The four topographic FB subdivisions (CTX, CNU, TH, and HY; Fig. 1*A*) are separated for clarity. SS1 is illustrated, and SS2 is its mirror image in the left FB. SS1 has two topologically distinct children subsystems, SS1.1 (shades of cyan) and SS1.2 (shades of red), each of which is subdivided further (see key for *A* and *B* in upper left and fully labeled hierarchy in Figs. 5 and 6 and Dataset S4 *C* and *E*). The yellow line in *A* outlines the cortical subplate, including the claustrum; regions caudal to FB in *B* (atlas levels 39 and 44) are white. For high-resolution details (not all regions are labeled) and further explanation of the flat map and atlas levels 3 to 44 (rostral to caudal) (see refs. 9 and 28). Atlas Levels adapted from ref. 28, which is licensed under CC BY 4.0. Complete abbreviation list of anatomical regions is in Dataset S1.

it is most closely associated with the lowest-level gustatory subsystem in the structure–function hierarchy, a default hypothesis is that the PL–MDm subsystem also has a primary (although not exclusive) gustatory function—an argument in principle similar to that used in proteomics analyses.

One level up the hierarchy is the set of regions that interconnect most densely the lowest-level GU and PL subsystems (*SI Appendix*, Fig. S2 *A* and *E*). By definition, this set contains all 13 regions in GU and PL, and 31 of the possible 44 connections (GU > PL and PL > GU) are formed (Dataset S4 *C*, *E*, and *F*). Considering the function associated above with the GU and PL subsystems, the higher-level inter-GU–PL subsystem may also be associated primarily with gustation (Fig. 5). The subsystem including GU, PL, and inter-GU–PL, with its 13 regions and 110 of a possible 156 connections between them, is shown in *SI Appendix*, Fig. S2*H*.

This bottom-up approach generates multilevel testable hypotheses. First, if a subsystem is assigned a provisional function based on a functional association for one or more of its regions, then other regions within the same subsystem, regardless of what is known about their function, may be hypothesized to contribute holistically to the subsystem functionality. Second, if a parent

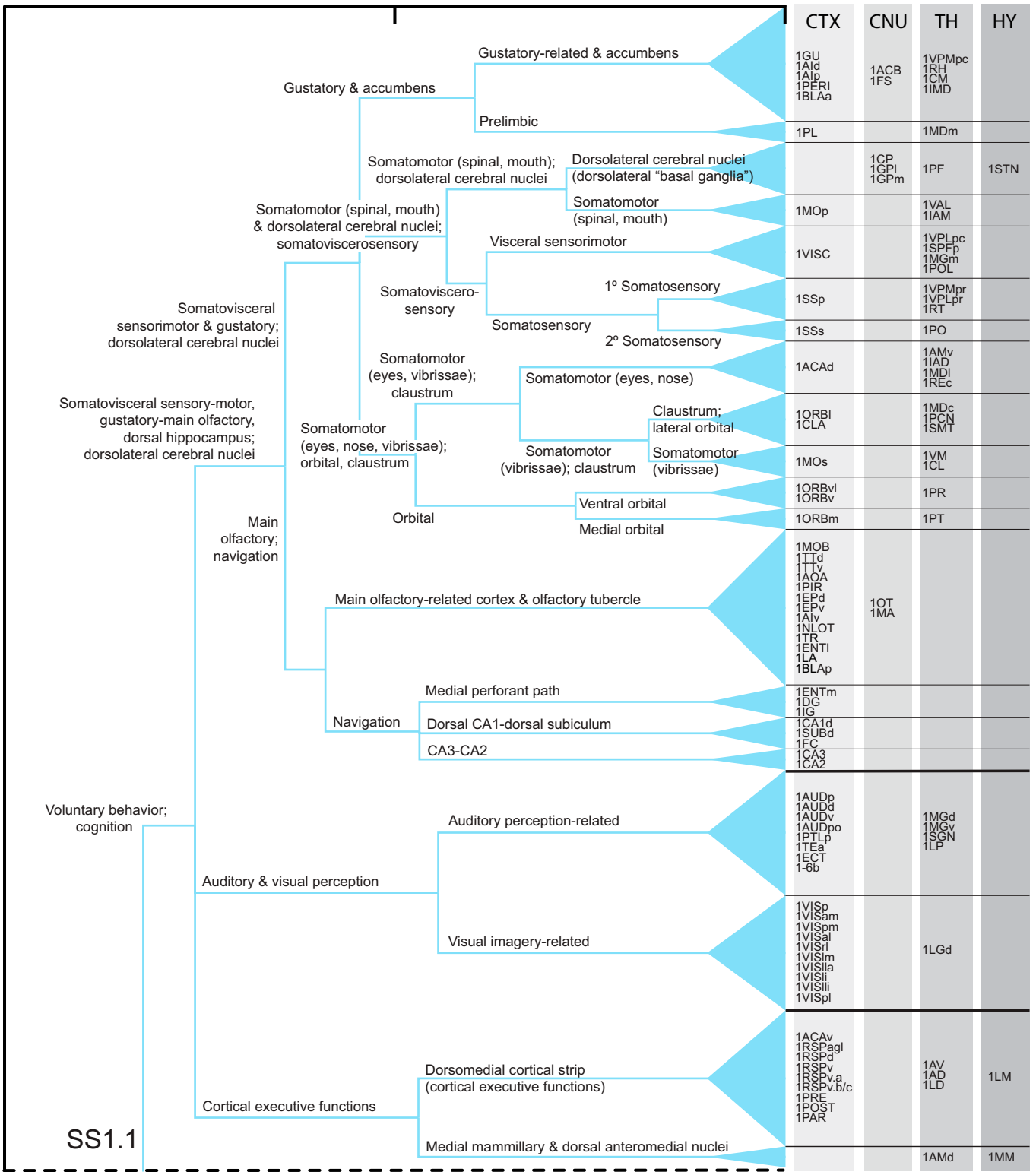

Fig. 5. Structure–function model of the subsystem hierarchy associated with upper-level FB2f subsystem, SS1.1 (Figs. 2 and 4 and Dataset S4 *C*, *E*, and *H*). Only the most obvious and least controversial functions are attributed to lowest-level subsystems (20 for SS1.1), and these functions propagate up the hierarchy as they combine with other subsystems and become more general. Overall, current evidence suggests that SS1.1 (and mirror image SS2.1) is primarily associated with voluntary behavior control and cognition. For clarity, the gray matter regional composition of each subsystem is divided into four categories: CTX, CNU, TH, and HY. Region order in bottom-level subsystems is random. A complementary analysis of SS1.2 follows in Fig. 6. Abbreviations are in Dataset S1.

subsystem has two children with distinct functional attributes, then the parent subsystem may be hypothesized to possess both attributes. Third, and similarly, if a parent subsystem has two children, one with a clear functional attribution and one without, then the parent subsystem may be hypothesized to possess the known and unknown functions of its children. Starting with the

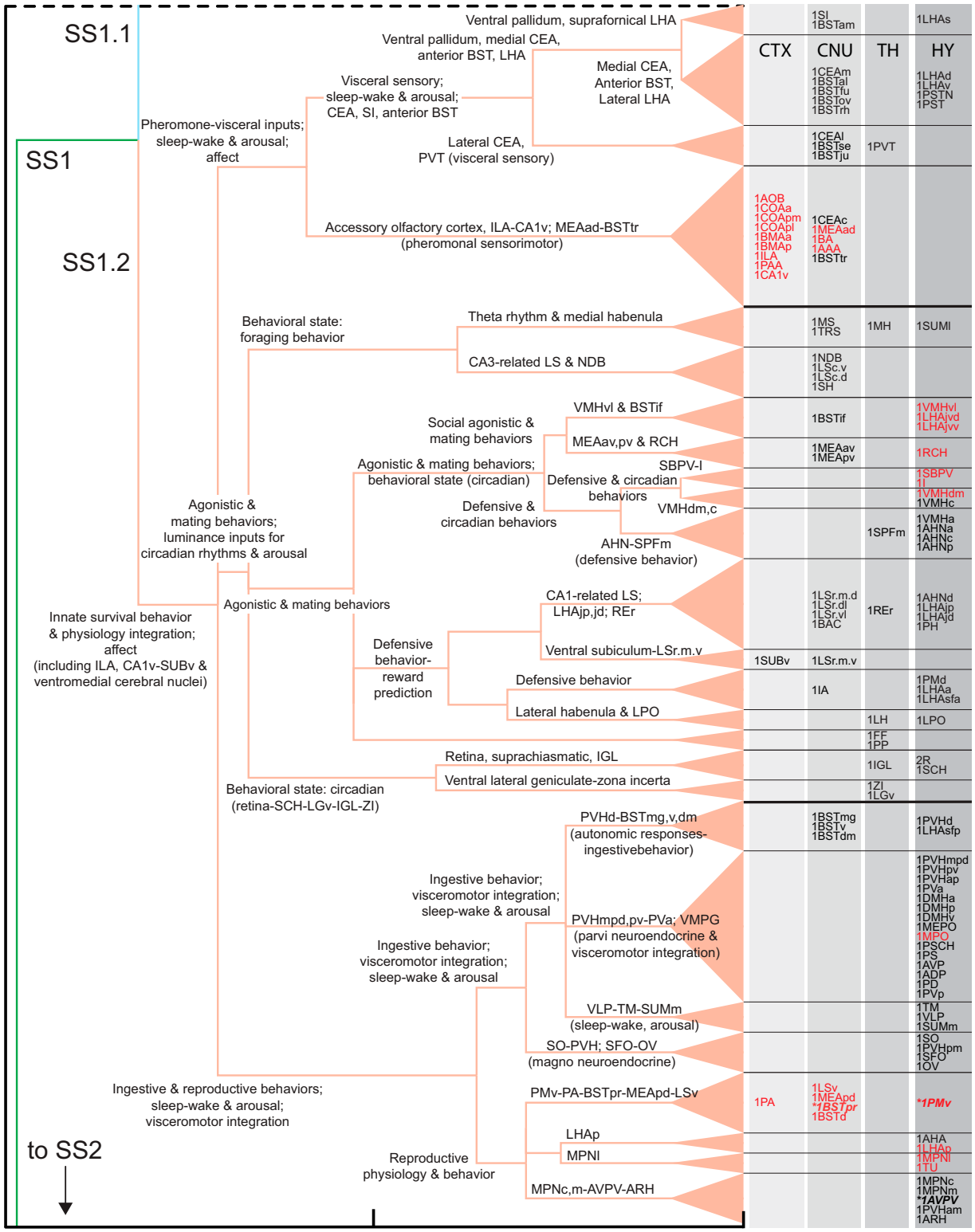

Fig. 6. Structure–function model of the subsystem hierarchy associated with upper-level FB2 subsystem, SS1.2 (shown in Figs. 2*C* and 4 and Dataset S4 *C*, *E*, and *H*), complementary to and following the similar analysis of SS1.1 in Fig. 5. SS1.2 (and its mirror image SS2.2) has 26 lowest-level subsystems, and overall, current evidence suggests it is primarily associated with the control of innate survival behaviors and their integration with physiologically appropriate visceral (autonomic and neuroendocrine) responses, accompanied by affect. Red abbreviations indicate the most sexually dimorphic regions measured as a difference in coclassification index (see *Comparing Female and Male Subsystem Hierarchies* and *SI Appendix*, Fig. S3*B*; all are in SS1.2 and mirror image SS2.2); bold italic abbreviations with asterisks are part of the sexually dimorphic connections BSTp > AVPV and BSTp > PMd. Abbreviations are in Dataset S1.

example in *SI Appendix*, Fig. S2, the entire structure–function hierarchy for FB2f (Figs. 5 and 6) can be analyzed in this way, combined with hierarchy subsystem stability (Fig. 2, fourth column) and intersubsystem WCD metrics (Fig. 3).

Top-Down Overview of FB Structure–Function Organization. Basic principles of intra-FB subsystem organization emerged after a bottom-up structure–function hierarchy was constructed. The evidence supports a model with relatively independent right and left FB sides (Fig. 3 *A* and *B*), each divided into two partly interacting subsystems (Figs. 3 and 5–7). One subsystem, which is centered in HY with relatively small components in ventromedial CTX and ventromedial CNU, is associated with the control of innate or instinctive survival behaviors (for example, ingestive; agonistic, aggressive and defensive; reproductive, sexual and parental; and locomotor), their integration with appropriate visceral (autonomic and neuroendocrine) responses, and affect. The other subsystem, which is centered in dorsolateral CTX, dorsolateral CNU, and dorsal TH, is associated with control of voluntary behavior and accompanying cognition. A complex array of specific connections between these two high-level subsystems (Fig. 3*B* and Dataset S4 *C*, *E*, and *H*) permits voluntary modulation of instinctive behavior expression and the latter to influence voluntary control of behavior in general. However, the densest connections between voluntary and innate behavior systems are associated with olfactory (main and accessory), gustatory, and visceral information processing. These functional inferences emerge from the ratio of intrinsic:extrinsic WCDs (intrinsic:extrinsic connection index): the ratio of intrinsic:extrinsic WCDs for SS1 and SS2 is 12.7:1 (Fig. 3*A*), whereas that for SS1.1 and SS1.2 (and their mirror image) is 6.8:1 within SS1 and 6.6:1 when connections between SS1 and SS2 are included (Fig. 3*B*).

Each high-level FB subsystem divides into three subsystems (Figs. 5–7). For the voluntary behavior control parent subsystem, the first child subsystem deals with cerebral somatovisceral, gustatory, and olfactory sensorimotor functions and with navigation control; at the next lower hierarchy level, main olfactory and navigation functions split from the others (and then they split). The second child subsystem deals with auditory and visual perception, and it in turn splits into auditory and visual perception-related subsystems. The third child subsystem is more difficult to characterize functionally; it is somewhat loosely associated with default mode network components tentatively assigned to cortical executive functions. Overall, then, the FB voluntary behavior subsystem supports cerebral hemisphere sensorimotor integration that in turn informs cerebral cortical navigation and other executive functions.

For the innate survival behavior and physiology integration parent subsystem, the first of three child subsystems subserves pheromonal and visceral information on one hand and sleep–wake and arousal components of behavioral state control on the other hand. The second child subsystem deals with luminance inputs and their influence on circadian rhythms and arousal and with agonistic and reproductive behaviors. The third child subsystem is involved primarily in three functional realms: 1) ingestive and reproductive behaviors, 2) sleep–wake and arousal aspects of behavioral state control, and 3) the integration generally of visceromotor (autonomic and neuroendocrine) responses. Overall, the FB innate survival subsystem supports hypothalamic mechanisms controlling 1) basic survival behaviors common to all animals (ingestive, agonistic, and reproductive), 2) behavioral state, and 3) the integration of appropriate visceromotor (autonomic and neuroendocrine) responses with the expression of specific survival behaviors under specific behavioral state conditions.

Combining the bottom-up and top-down approaches provides a complete view of FB subsystem arrangement at all structure–function hierarchy levels illustrated in Figs. 5 and 6. Specific connections established within each subsystem, and specific connections established between any pair of subsystems, can be determined most easily by exploring the interactive graphics tool provided in Dataset S4. Topographically, regions forming the top three hierarchy levels tend to aggregate spatially, with the voluntary behavior control subsystem lying dorsolaterally and the innate survival integration subsystem lying ventromedially in the FB (Figs. 4*B* and 7*B*). Since the late 19th century (29–31), these two FB compartments have been associated in vertebrates generally with two major longitudinal fiber tracts, the lateral FB bundle (called internal capsule in mammals) and medial FB bundle (Fig. 7)—or more generally with the lateral and medial FB bundle systems (32). Thus, the top, most general cluster tree level may reflect the genetic program for the development and adult form of the vertebrate NS wiring diagram.

A **Forebrain structure-function subsystems (upper levels)**

1.1 Voluntary behavior control: cognition (lateral forebrain subsystem)
- 1.1.1 Somatovisceral, gustatory, & olfactory sensorimotor with dorsolateral cerebral nuclei; navigation
  - 1.1.1.1 Somatovisceral & gustatory sensorimotor; dorsolateral cerebral nuclei
  - 1.1.1.2 Main olfactory; navigation
- 1.1.2 Auditory-visual perception-related
  - 1.1.2.1 Auditory perception-related
  - 1.1.2.2 Visual perception-related
- 1.1.3 Cortical executive functions

1.2 Innate survival behavior & physiology integration: affect (medial forebrain subsystem)
(including ILA, CA1v-SUBv & ventrolateral cerebral nuclei)
- 1.2.1 Pheromonal-visceral inputs; sleep-wake & arousal
  - 1.2.1.1 Visceral sensory; sleep-wake & arousal
  - 1.2.1.2 Pheromonal sensorimotor
- 1.2.2 Agonistic & reproductive behaviors; luminance inputs: circadian rhythms & arousal;
- 1.2.3 Ingestive & reproductive behaviors; sleep-wake & arousal; visceromotor integration

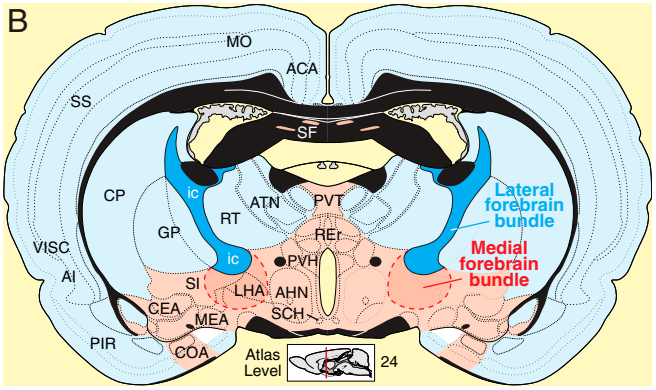

Fig. 7. Summary of rat FB upper-level structure–function subsystem model. (*A*) Tabular overview of the central interpretative hypothesis emerging from subsystem structure–function hierarchy analysis. (*B*) Spatial distribution of the voluntary behavior–lateral FB subsystem (blue) and innate survival–medial FB subsystem (red) illustrated on a transverse map through a mid-rostrocaudal FB level. See *Top-Down Overview of FB Structure–Function Organization* and Figs. 4–6 for details. Atlas Level template from ref. 9, which is licensed under CC BY 4.0. Abbreviations are in Dataset S1.

Comparing Female and Male Subsystem Hierarchies. The two sexually dimorphic connections in SS1.2 (and mirror image SS2.2; BSTpr > AVPV, BSTpr > PMv) produce remarkably widespread

differences between the FB2f and FB2m network attributes, even when connection weights in a subsystem are identical. First, a difference matrix for the two coclassification matrices (Fig. 2, third column) shows subtle differences in the coclassification index (a measure of coherence within the network) for 34% of the FB2 regions, which are concentrated ipsilaterally and in SS1.2 and SS2.2, the medial FB subsystem (Fig. 8*A* and Dataset S4 *C*, *E*, and *I*). Second, regions with the greatest differences were rank-ordered, with the top 20th percentile comprising 28 regions, all in the medial FB subsystem (*SI Appendix*, Fig. S3 *A* and *B*). The BSTpr ranks first, with the top 7 regions in the reproductive behavior and physiology subsystem and 10 of the next 11 regions in the pheromone sensorimotor subsystem. The remaining regions are members of these two subsystems and of those also involving agonistic behaviors, circadian mechanisms, and visceromotor integration (Figs. 5 and 6 and Dataset S4 *C*, *E*, and *I*). Third, direct comparison of the FB2f and FB2m MRCC hierarchies reveals two separate clusters of differences at the bottom subsystem level in SS1.2 (and mirror image SS2.2; *SI Appendix*, Fig. S3*C*) that are directly involved in reproductive, agonistic, and circadian behaviors and physiology (Dataset S4 *C*, *E*, and *I*). One cluster (*SI Appendix*, Fig. S3*D*) involves the same set of seven regions, but a subsystem border rearrangement produces three subsystems in female and two in male and changes parent relationships in the hierarchy. The other cluster involves four identical subsystems (*SI Appendix*, Fig. S3*E*) in a reordered sequence that also changes their parent relationships in the hierarchy. The most obvious functional significance of this reordering is that in females and males, the sexually dimorphic AVPV, which is critical for ovulation, is in different subsystems with different parent relationships (*SI Appendix*, Fig. S3*E*). Overall, the FB2m hierarchy has 164 subsystems, compared to 166 for FB2f (above), and they share 146 subsystems in common (73 in SS1 and 73 in mirror image SS2).

Global Network Features. The intra-FB connectome was analyzed for three basic network attributes. First, network centrality suggests the relative importance of regions (nodes), the most central being called hubs. The mirror image SS1 and SS2 each have 11 hubs (Fig. 9); CTX has 7 in two spatially continuous clusters, one caudally involving the lateral entorhinal (ENTl) and perirhinal (PERI) areas and the other rostrally involving prefrontal, orbital, and supplementary motor areas. TH has three hubs clustered in the midline group, and HY has just one hub, the posterior hypothalamic nucleus. The possible functional significance of these 11 regions can be gleaned from Figs. 5 and 6 [also see *Computational (Virtual) Lesions Relevant for Alzheimer's Disease and Depression*]. Second, the term "rich club" refers to a set of individually highly connected and mutually highly interconnected nodes, and analysis shows an identical set of four innermost circle members in SS1 and SS2 (Fig. 9). CTX has one (prefrontal infralimbic area [ILA]), and HY has the other three (posterior hypothalamic and histaminergic tuberomammillary nuclei and lateral hypothalamic area anterior region). A functional interpretation of this intriguing and unexpected bilateral quartet restricted to the medial FB subsystem is not immediately apparent. Third, "small-world" applies to networks with highly clustered nodes connected by short paths, and notably, the FB2 subsystem shows stronger small-world organization than any of its subconnectomes considered alone, including CTX (*SI Appendix*, Fig. S4).

Computational (Virtual) Lesions Relevant for Alzheimer's Disease and Depression. Changing a brain network's anatomical coverage by adding or subtracting subconnectomes composed of connections within one side and/or between sides, commonly shifts rankings of putative hubs (18, 22), which applies to FB2 and its subconnectomes (*SI Appendix*, Fig. S5). Above we showed that two very sexually dimorphic connections arising from a single region (BSTpr; in SS1 and mirror image SS2) produce clearly dimorphic FB networks in male and female rats. Here we test computationally the hypothesis that making a strong local change (lesioning rich club or hub regions by removing all their incoming and outgoing connections) also has quantifiable effects on network organization. One test targeted the medial temporal CTX domain, ENTl-PERI (Fig. 9). Only these two spatially adjacent regions exhibit hub stability across the FB2 subconnectome and all of its relevant subconnectomes (*SI Appendix*, Fig. S5), and the presumed homolog of this rat hub domain, which has been called the entorhinal–perirhinal border zone (33), shows the earliest signs of tauopathy in Alzheimer's disease. The other test targeted the ventral prefrontal ILA, the only CTX rich club member, which is also a hub (Fig. 9); bilateral deep brain stimulation implicates a zone in or around the presumed human homolog as one region of interest in clinical depression (34).

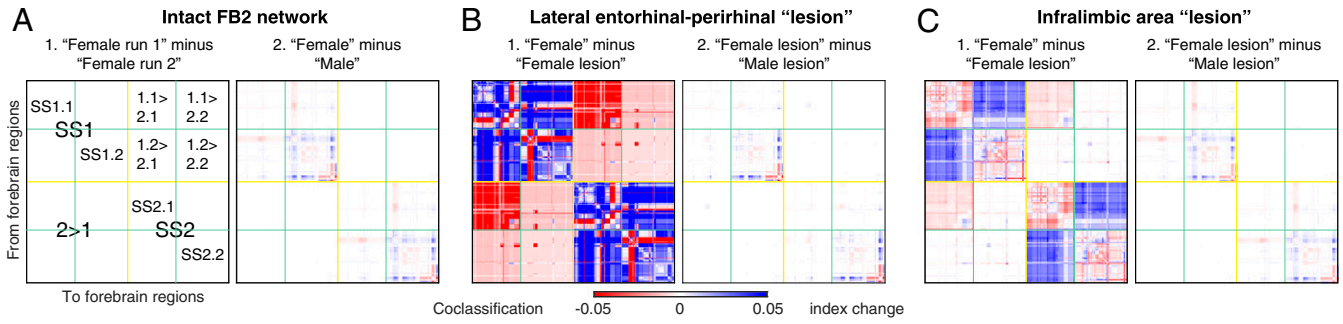

Fig. 8. Comparison of coclassification difference matrices for female and male FB2 networks and for intact vs. Alzheimer's lesion or depression lesion. In all panels, positive differences (displayed in blue) indicate greater coclassification in the first (minuend) over the second (subtrahend) matrix element. To allow comparison, all difference matrices are displayed in the same canonical FB2f ordering scheme (Fig. 2). (*A*) As a control (*A*, *1*), the original FB2f matrix (Fig. 2, third column) was run twice (each with 2.5 million uniformly sampled partitions); negligible differences were found between the two replicates (for quantification, see *SI Appendix*, Table S1). The 99th percentile of differences between these replicates was taken as a significance threshold, applied to all other comparisons between sexes and lesions (below-threshold differences are discarded). (*A*, *2*) Coclassification differences obtained by subtracting male matrix from female matrix. (*B*) Effects of ENTl-PERI numerical lesions (in SS1 and SS2) in the female (*B*, *1*) and a comparison with the effects in male (*B*, *2*). The index plotted in *B*, *1*, expresses the change in a region pair's coclassification that may be higher in the intact (blue) or higher in the lesioned (red) network configuration; the sex difference index for *B*, *2*, corresponds to that for *A*, *2*. (*C*) Effects of ILA numerical lesions (in SS1 and SS2) in the female (*C*, *1*) and a comparison with the effects in male (*C*, *2*). Coclassification index measures correspond to those shown in *B*, *1*, and *B*, *2*. For the intact FB2f and FB2m coclassification matrices and associated subsystem hierarchies, see Figs. 2, 5, and 6; *SI Appendix*, Fig. S3 *C–E*; and Dataset S4. For quantitation of matrix differences, see *SI Appendix*, Table S1.

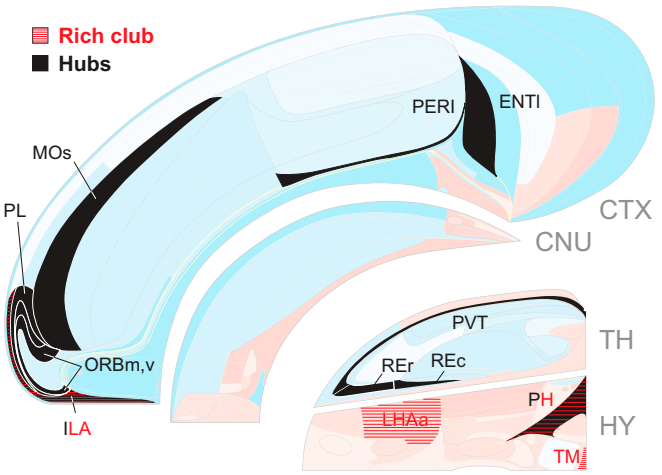

Fig. 9. Spatial distribution of candidate hubs and rich club innermost circle regions (nodes) for the FB2 network on a right FB flat map (Figs. 1*A* and 4). The left FB has a mirror image set of hubs and rich club members, and the results are identical for female and male rats. Only two regions (ENTl and the adjacent PERI) maintain their status as hubs when smaller FB divisions (CTX1/2 and EB1/2) containing them are considered by themselves (*SI Appendix*, Fig. S5). For the rich club, out of 425 tests, 256 are significant using a false discovery rate of 0.001 (adjusted for independent or positively dependent tests). See *Global Network Features* for details and Dataset S1 for abbreviations.

The most obvious results (details in Fig. 8 *B* and *C*; *SI Appendix*, Table S1; and Dataset S4) show first that globally, both highly localized lesions have widespread effects, reverberating through nearly all (96 to 98%) node pair associations as measured by above-chance changes in coclassification index, although the absolute sum of changes is ∼3.5× greater for the two-region (ENTl–PERI) lesion. These changes tend to strengthen coclassification among region pairs, increasing overall FB2 network coherence. Second, at the top hierarchy level (right and left sides; SS1 and SS2), both lesions decrease intrasubsystem coherence (blue in Fig. 8) while increasing intersubsystem (SS1 > SS2, SS2 > SS1) coherence (red in Fig. 8). Third, a strikingly differential pattern of lesion effects (symptoms) occurs at the next hierarchy level (SS1.1 or lateral FB subsystem, SS1.2 or medial FB system, and mirror images). ENTl–PERI lesion effects are relatively uniformly distributed through SS1 (SS1.1, SS1.2), whereas the ILA lesion produces a checkerboard pattern, with network coherence increased in the lateral and medial FB subsystems and decreased in the interactions between them (Fig. 8 *C*, *1*). Fourth, both lesions do not significantly alter sexually dimorphic network features (Fig. 9 *B*, *2*, and *C*, *2*), which remain similar to the dimorphisms in intact female and male FB networks (Fig. 8 *A*, *2*). Fifth, overall, the ENT-PERI–lesioned FB2f network shares only 32 subsystems with the intact network (with 166 subsystems), whereas the ILA-lesioned fB2f network shares even fewer subsystems (26) with the intact network. Focal simulations like these may be helpful in designing animal models of mental health disorders and interpreting the complex and widespread neuropathology associated with the underlying neural networks.

Connection Sign. All FB region macroconnections were associated with a provisional sign—excitatory, inhibitory, or excitatory and inhibitory neurotransmission (glutamatergic, GABAergic, or both, respectively), based on current literature and reservations about their usefulness as markers (*SI Appendix*, *Materials and Methods*). The results show (Dataset S4 *C*, *E*, and *P*) a clear dichotomy at the second hierarchy level: glutamatergic macroconnections are heavily favored in the lateral FB subsystem (SS1.1) and GABAergic connections predominate in the medial FB subsystem (SS1.2). Considering the 46 lowest-level subsystems in parent SS1, 20 are exclusively glutamatergic, none are exclusively GABAergic, and 26 use both; 16 exclusively glutamatergic subsystems are in SS1.1 whereas all SS1.2 lowest-level subsystems use both. Recall that regional interneurons are not considered in this macrolevel network analysis. The exclusively glutamatergic corticothalamic subsystems in SS1.1 may be especially prone to hyperexcitability with decreased inhibitory interneuron tone (as in epilepsy).

Discussion

Because nervous system function is determined by nervous system structure (8, 13), the hierarchical subsystem model presented here can be a powerful hypothesis-generating engine for experimental systems neuroscience research. Mechanistic explanations of nervous system function can no longer ignore network complexity—the FB macroconnectome alone has over 35,000 connections, with its regions averaging 77 output (and 77 input) connections with other regions—but the hierarchical subsystem model provides a conceptual framework for navigating this complexity. In fact, starting at any region (node) in the hierarchy leads eventually to any other region, through one or more paths, each with one or more connections—sequences that can be established most unambiguously with systematic application of experimental monosynaptic axonal pathway tracing strategies (35).

This work has four main limitations. First, the structural data can always improve to yield more refined hierarchical subsystem models; version 1.0 is a starting point for the iterative data > modeling > data cycle used to clarify organizing principles of any complex system (36). Second, our top-level macroneuroscience approach provides boundary conditions for overall interregional connection organization, but finer, nested analysis levels based on neuron types and single neurons (with axon branching patterns and synapse distribution) are needed to explain how intraregional input–output transformations are generated. Third, network properties described here apply to intrinsic circuitry of a major nervous system part (FB), but they depend on anatomical coverage and do not stabilize until considered within the entire nervous system network (ref. 12 and *SI Appendix*, Fig. S5). Fourth, our static model should be superseded by a dynamic model that includes synaptic strengths under physiological conditions and external factors such as the influence of glia and hormones.

Two core hypotheses underlie our analysis: the FB is one of three primary structure–function subdivisions of the vertebrate brain (1, 2), and gray matter region sets more densely connected with each other than with other sets have a unique functional identity (22). MRCC analysis revealed a sexually dimorphic hierarchical model of intra-FB structure–function subsystems with 2 subsystems at the top and 92 or 90 at the bottom of the cluster tree in female and male, respectively. At a macrolevel analysis, the subsystem organization is presumably species-specific and reflects hard-wired biases of information flow through the network, determined by genetic programs assembling the circuitry during embryogenesis (17, 23). The upper subsystem hierarchy levels are remarkably simple. The top level has two mirror image subsystems, and for each subsystem all regions (except the retina) are on one side of the brain. Thus, at the top level the FB network consists essentially of right and left sides that are relatively independent (intrasubsystem connections >12× heavier than intersubsystem connections).

Then, each top-level subsystem is divided into two mirror image second-level subsystems that are distinct structurally and functionally (Fig. 7). One subsystem lies dorsolaterally and is associated with voluntary behavior control and cognition, whereas the other subsystem lies ventromedially and is associated with innate survival mechanisms and affect. This dichotomous structure–function

network partition is supported by two lines of evidence. First, dorsolateral and ventromedial structural FB domains in vertebrates have long been associated with two major longitudinal tracts or axon bundles, the lateral and medial FB bundles, respectively (29–31), suggesting the subsystem dichotomy is fundamental and ancient. Second, functional studies in mammals demonstrate that transection between FB and midbrain (separating FB from the remaining nervous system) tends to eliminate spontaneous behavior (3, 4), whereas more rostral transection leaving HY and immediately surrounding regions intact allows the spontaneous expression of at least some survival behaviors and physiological responses, although they tend to be undirected or reflex in nature (3, 4, 37). The dorsal TH and CTX must remain intact for directing and prioritizing behaviors generally and for utilizing past experience (4). In addition to these cognitive functions, it has been common since Woodworth and Sherrington (38) to ascribe emotional (affective) consciousness to CTX, relegating coordinated pseudo-affective reflexes to HY and related brainstem regions (37). However, the cortical regions indicated here to be most directly related to affect also have substantial direct connections to the HY: infralimbic area, ventral hippocampus, and cortical amygdalar area (Dataset S2).

The main goals of this theoretical macroneuroscience project are to expand anatomical coverage to the nervous system as a whole and to provide an expanded network analysis toolbox for community utilization of our systematic and comprehensive connectional database. However, the results so far suggest that structure–function connectional subsystems may be fruitful targets for exploring genetic programs in brain development and for targeting therapeutic interventions in mental health disorders.

Materials and Methods

All connection report collation and network analysis methods were described previously (12, 16, 18–22) and are summarized and updated in *SI Appendix, Materials and Methods*.

Data Availability. Connection report metadata are in a Microsoft Excel spreadsheet (Dataset S2), as are data from the reports used for connection matrices (Dataset S3). Searchable connection report data are freely available at The Neurome Project (https://sites.google.com/view/the-neurome-project/home). Network analyses were done on the FB2 connection matrix (Dataset S3, worksheet "FB2 topographic bins") with tools collected in the Brain Connectivity Toolbox (https://sites.google.com/site/bctnet/). All study data are included in the article and supporting information.

1. W. J. H. Nauta, M. Feirtag, *Fundamental Neuroanatomy* (Freeman, New York, 1986).
2. L. W. Swanson, What is the brain? *Trends Neurosci.* **23**, 519–527 (2000).
3. J. C. Hinsey, S. W. Ranson, R. F. McNattin, The rôle of the hypothalamus and mesencephalon in locomotion. *Arch. Neurol. Psychiatry* **23**, 1–43 (1930).
4. H. J. Grill, R. Norgren, Neurological tests and behavioral deficits in chronic thalamic and chronic decerebrate rats. *Brain Res.* **143**, 299–312 (1978).
5. E. Stellar, The physiology of motivation. *Psychol. Rev.* **61**, 5–22 (1954).
6. L. W. Swanson, G. J. Mogenson, Neural mechanisms for the functional coupling of autonomic, endocrine and somatomotor responses in adaptive behavior. *Brain Res.* **228**, 1–34 (1981).
7. L. W. Swanson, Cerebral hemisphere regulation of motivated behavior. *Brain Res.* **886**, 113–164 (2000).
8. P. T. Young, *Motivation and Emotion: A Survey of the Determinants of Human and Animal Activity* (John Wiley & Sons, New York, 1961).
9. L. W. Swanson, Brain maps 4.0-Structure of the rat brain: An open access atlas with global nervous system nomenclature ontology and flatmaps. *J. Comp. Neurol.* **526**, 935–943 (2018).
10. O. Sporns, *Networks of the Brain* (MIT Press, Cambridge, MA, 2011).
11. L. G. S. Jeub, O. Sporns, S. Fortunato, Multiresolution consensus clustering in networks. *Sci. Rep.* **8**, 3259 (2018).
12. L. W. Swanson, J. D. Hahn, L. G. S. Jeub, S. Fortunato, O. Sporns, Subsystem organization of axonal connections within and between the right and left cerebral cortex and cerebral nuclei (endbrain). *Proc. Natl. Acad. Sci. U.S.A.* **115**, E6910–E6919 (2018).
13. J. G. White, E. Southgate, J. N. Thomson, S. Brenner, The structure of the nervous system of the nematode *Caenorhabditis elegans. Philos. Trans. R. Soc. Lond. B Biol. Sci.* **314**, 1–340 (1986).
14. S. J. Cook *et al.*, Whole-animal connectomes of both *Caenorhabditis elegans* sexes. *Nature* **571**, 63–71 (2019).
15. E. C. Friedberg, *Sydney Brenner: A Biography* (Cold Spring Harbor Laboratory Press, Cold Spring Harbor, NY, 2010).
16. M. Bota, O. Sporns, L. W. Swanson, Architecture of the cerebral cortical association connectome underlying cognition. *Proc. Natl. Acad. Sci. U.S.A.* **112**, E2093–E2101 (2015).
17. L. W. Swanson, J. W. Lichtman, From Cajal to connectome and beyond. *Annu. Rev. Neurosci.* **39**, 197–216 (2016).
18. L. W. Swanson, O. Sporns, J. D. Hahn, Network architecture of the cerebral nuclei (basal ganglia) association and commissural connectome. *Proc. Natl. Acad. Sci. U.S.A.* **113**, E5972–E5981 (2016).
19. L. W. Swanson, J. D. Hahn, O. Sporns, Organizing principles for the cerebral cortex network of commissural and association connections. *Proc. Natl. Acad. Sci. U.S.A.* **114**, E9692–E9701 (2017).
20. L. W. Swanson, O. Sporns, J. D. Hahn, The network organization of rat intrathalamic macroconnections and a comparison with other forebrain divisions. *Proc. Natl. Acad. Sci. U.S.A.* **116**, 13661–13669 (2019).
21. J. D. Hahn, O. Sporns, A. G. Watts, L. W. Swanson, Macroscale intrinsic network architecture of the hypothalamus. *Proc. Natl. Acad. Sci. U.S.A.* **116**, 8018–8027 (2019).
22. L. W. Swanson, O. Sporns, J. D. Hahn, The network architecture of rat intrinsic interbrain (diencephalic) macroconnections. *Proc. Natl. Acad. Sci. U.S.A.* **116**, 26991–27000 (2019).
23. L. W. Swanson, M. Bota, Foundational model of structural connectivity in the nervous system with a schema for wiring diagrams, connectome, and basic plan architecture. *Proc. Natl. Acad. Sci. U.S.A.* **107**, 20610–20617 (2010).
24. R. A. Brown, L. W. Swanson, Neural systems language: A formal modeling language for the systematic description, unambiguous communication, and automated digital curation of neural connectivity. *J. Comp. Neurol.* **521**, 2889–2906 (2013).
25. L. W. Swanson, *Neuroanatomical Terminology: A Lexicon of Classical Origins and Historical Foundations* (Oxford University Press, Oxford, 2015).
26. L. W. Swanson, P. R. Hof, A model for mapping between the human and rodent cerebral cortex. *J. Comp. Neurol.* **527**, 2925–2927 (2019).
27. G. Gu, A. Cornea, R. B. Simerly, Sexual differentiation of projections from the principal nucleus of the bed nuclei of the stria terminalis. *J. Comp. Neurol.* **460**, 542–562 (2003).
28. J. D. Hahn *et al.*, An open access mouse brain flatmap and upgraded rat and human brain flatmaps based on current reference atlases. *J. Comp. Neurol.*, 10.1002/cne.24966 (2020).
29. L. Edinger, *Vorlesungen über den Bau der nervösen Centralorgane des Menschen und der Thiere. Für Ärzte und Studirende* (F. C. W. Vogel, Leipzig, 1983).
30. E. S. Gurdjian, The diencephalon of the albino rat. *J. Comp. Neurol.* **43**, 1–114 (1927).
31. W. J. H. Nauta, W. Haymaker, "Hypothalamic nuclei and fiber connections" in *The Hypothalamus*, W. Haymaker, E. Anderson, W. J. H. Nauta, Eds. (C. C Thomas, Springfield, 1969), pp. 136–209.
32. L. W. Swanson, *Brain Maps: Structure of the Rat Brain* (Elsevier, Amsterdam, 1992).
33. S. A. Small, L. W. Swanson, A network explanation of Alzheimer's regional vulnerability. *Cold Spring Harb. Symp. Quant. Biol.* **83**, 193–200 (2018).
34. P. Riva-Posse *et al.*, Rapid antidepressant effects of deep brain stimulation and their relation to surgical protocol. *Biol. Psychiatry* **88**, e37–e39 (2020).
35. R. H. Thompson, L. W. Swanson, Hypothesis-driven structural connectivity analysis supports network over hierarchical model of brain architecture. *Proc. Natl. Acad. Sci. U.S.A.* **107**, 15235–15239 (2010).
36. A. Rosenblueth, N. Wiener, The role of models in science. *Philos. Sci.* **12**, 316–321 (1945).
37. P. Bard, On emotional expression after decortication with some remarks on certain theoretical views, parts I and II. *Psychol. Rev.* **41**, 309–329, 424–449 (1934).
38. R. S. Woodworth, C. S. Sherrington, A pseudaffective reflex and its spinal path. *J. Physiol.* **31**, 234–243 (1904).